Biochemistry and Biophysics Reports 4 (2015) 98–103

Contents lists available at ScienceDirect

Biochemistry and Biophysics Reports

journal homepage: www.elsevier.com/locate/bbrep

Immobilization of *Bacillus subtilis* oxalate decarboxylase on a Zn-IMAC resin

Umar Twahir [a], Laura Molina [a], Andrew Ozarowski [b], Alexander Angerhofer [a,*]

[a] Department of Chemistry, University of Florida, Gainesville, FL 32611-7200, USA
[b] National High Magnetic Field Laboratory, Florida State University, Tallahassee, FL 32310, USA

ARTICLE INFO

Article history:
Received 16 July 2015
Received in revised form
19 August 2015
Accepted 24 August 2015
Available online 28 August 2015

Keywords:
Oxalate decarboxylase
OxDC
IMAC
Electron paramagnetic resonance
EPR

ABSTRACT

Oxalate decarboxylase, a bicupin enzyme coordinating two essential manganese ions per subunit, catalyzes the decomposition of oxalate into carbon dioxide and formate in the presence of oxygen. Current efforts to elucidate its catalytic mechanism are focused on EPR studies of the Mn. We report on a new immobilization strategy linking the enzyme's N-terminal His_6-tag to a Zn-loaded immobilized metal affinity resin. Activity is lowered somewhat due to the expected crowding effect. High-field EPR spectra of free and immobilized enzyme show that the resin affects the coordination environment of the active site Mn ions only minimally. The immobilized preparation was used to study the effect of varying pH on the same sample. Repeated freeze-thaw cycles lead to break down of the resin beads and some enzyme loss from the sample. However, the EPR signal increases due to higher packing efficiency on the sample column.

1. Introduction

Oxalate Decarboxylase (OxDC) isolated from *Bacillus subtilis* is a member of the cupin superfamily of proteins, characterized by a series of conserved residues that form β-barrels supporting the binding of a range of metal-cofactors [1–3]. OxDC coordinates a manganese ion in each of its two cupin folds [4–6]. It catalyzes the heterolytic cleavage of the typically unreactive carbon–carbon bond of oxalic acid, yielding formate and carbon dioxide in the presence of dioxygen as a co-catalyst [7,8]. The enzyme also exhibits a minute oxidase activity (0.2% of all turnovers), producing another equivalent of carbon dioxide and hydrogen peroxide in the place of formate. The ability of the enzyme to carry out two chemically distinct catalytic reactions has garnered much interest in understanding its mechanistic pathway.

X-ray crystallography on OxDC points to the N-terminal manganese as the active site where bound product was observed and a flexible amino acid loop, SENS161-164, opens a solvent channel to the Mn ion that appears to be absent at the C-terminal binding site [5]. OxDC crystallizes as a hexamer, showing face-stacked dimers of trimers [4,5]. Less is known about the C-terminal Mn ion which is essential for catalysis, with proposals for it ranging from being a second active site [9] to merely serving a structural role [5]. Recent EPR (electron paramagnetic resonance) spin trapping experiments suggest that the C-terminal Mn might be the site of oxygen binding requiring a long range electron transfer between the N- and C-terminal sites to facilitate catalysis [10].

EPR has been used successfully to probe radical intermediates during turnover and observing different coordination environments of the two Mn ions [6,10–15]. The resting state oxidation number of the Mn ions is predominantly +2 [7,15,16]. High-field multi-frequency EPR provided evidence for pH dependent conformational changes as seen by changes in the Mn coordination environment [15]. Tabares et al. found two pH-dependent forms of the N-terminal Mn(II), site A (low pH) and B (high pH), and five different pH-dependent forms of the C-terminal Mn(II), sites H (high pH, >7.0), M (medium pH, 4.5–6.5), X (second intermediate pH range 5.5–7.5), plus L and L2 (low pH), below 4.5. More recent DFT and EPR studies on WT OxDC and the site-directed mutant W132F by Campomanes et al. confirmed the assignments made by Tabares et al. at high pH [11]. EPR experiments require large amounts of highly concentrated and pure enzyme in order to give the high signal-to-noise ratio needed for revealing subtle spectroscopic effects. An efficient *Escherichia coli* overexpression system yields high quality enzyme in good yields, yet more comprehensive data sets such as full pH or redox scans are still bottlenecked by enzyme production. This prompted us to develop a strategy for increasing the protein concentration through

* Correspondence to: University of Florida, Department of Chemistry, P.O.Box. 117200, Gainesville, FL 32611, USA. Fax: +1 3523920872.
E-mail address: alex@chem.ufl.edu (A. Angerhofer).

http://dx.doi.org/10.1016/j.bbrep.2015.08.017

immobilization on a metal affinity chromatography (IMAC) resin which also allows to reuse the same sample for multiple experiments.

IMAC resins are commonly used in protein purification using poly(His) tags on either the N- or C-terminus of the protein [17]. A variety of metals may be utilized for this purpose, primarily from the first transition metal series. Due to their Lewis acidity these metals will coordinate to the nitrogens of the His tag leading to chelation of the metal center by one or more histidines [18]. Other immobilization strategies using covalent linkages have also been used for proteins [19,20] and efforts have been reported before on immobilizing oxalate degrading enzymes for the purposes of clinical sensing and bioremediation of oxalate [21–23]. In particular, OxDC has been immobilized on Eupergit® C and the effects of pH and temperature on the kinetic parameters tested [24]. Immobilization on Eupergit® C leads to multiple attachment sites on the protein with various side chains of the protein amino acids. Lin et al. reported increased temperature stability of the immobilized protein from 55 °C to up to 70 °C, similar pH dependent activity profiles, a 27% decrease in k_{cat}, and a 37% increase in K_M compared to the free enzyme. The decrease in catalytic efficiency was attributed to the structural deformation of the protein due to adsorption on the resin.

Herein, we report on the use of the encoded His_6-tag to immobilize OxDC on a Zn-IMAC resin primarily for use in EPR studies requiring high enzyme concentrations. Zinc was chosen because it is diamagnetic. Precedence for the use of immobilized proteins and model systems for EPR studies exist in the literature [19,25–29]. We report on the catalytic activity, X-band and high-field EPR of the immobilized enzyme, as well as the use of a flow-system to allow for in situ changes of the buffer environment, and discuss the effects of immobilization.

2. Material and methods

2.1. Chemicals

The following chemicals were purchased from Fisher Scientific (Pittsburg PA, ACS Grade) and used as received without further purification: phosphoric acid, glacial acetic acid, sodium chloride, sodium phosphate, sodium acetate, sodium hydroxide, and tris (hydroxymethyl)aminomethane (Tris). Zinc sulfate was purchased from Sigma Aldrich (St. Louis, MO). Uncharged Profinity IMAC resin was purchased from Bio-Rad Laboratories (Hercules, CA). All solutions were prepared utilizing 18 MΩ•cm de-ionized water generated by a Thermo Scientific Barnstead Nanopure model 7134.

2.2. Expression and purification of OxDC

Expression and purification of recombinant His_6-tagged *B. subtilis* wild-type OxDC was carried out following previously published procedures [5–7,10,30]. To remove dissolved metals from the preparation, Chelex 100 resin (Bio-Rad, Hercules CA) was added to the enzyme after the serial dialysis steps. The solution was shaken for approximately 1 h following removal of the resin. The enzyme solution was then concentrated using Amicon Centriprep YM-30 centrifugal filter units (EMD Millipore, Billerica, MA). Concentrated enzyme samples (approximately 35–40 mg/mL) were stored as 200 μL aliquots in Eppendorf tubes at −80 °C until used for experiments.

2.3. Zn-IMAC preparation

IMAC columns were custom designed out of Kel-F to serve as cryogenic EPR sample containers (4 × 5 mm ID × OD, 5.46 cm length for X-band and 6.1 × 7.3 mm ID × OD, 3.3 cm length for high-field). A disk of polypropylene filter paper (5 μm particle size, Typar 3609L, Midwest Filtration LLC) with a diameter equal to the ID was fit tightly into the bottom of each column. Resin preparation was carried out following the Profinity™ IMAC Resin Manual. 250 μL of uncharged Resin (50/50 v/v resin and solvent was added to the column, washed for 15 min with 1% acetic acid, 0.12 M phosphoric acid for cleaning, followed by 10 column volumes of DI water. Further washing for another 15 min with 2 M NaCl removed ionic contaminants followed by rinsing with 10 column volumes of DI water. 10 column volumes of binding buffer (50 mM sodium phosphate, 0.3 mM NaCl at pH 8.0) was then flowed through the column, followed by 10 column volumes of 50 mM sodium acetate, 0.3 M NaCl, pH 4.0 to prepare for metal binding. Zn(II) ions were loaded onto the column by applying 5 column volumes of 0.3 M $ZnSO_4$, followed by 5 column volumes of 50 mM sodium acetate, 0.3 M NaCl, pH 4.0 and 10 column volumes of DI water to rinse. Finally, the column was equilibrated with starting buffer (50 mM Tris–HCl, 500 mM NaCl).

WT OxDC was loaded onto the column by passing 400 μL of 40 mg/ml free enzyme solution through the column. The flow-through solution was collected and passed through the column at least three times to capture as much His_6-tagged OxDC as possible. The column was then re-equilibrated with starting buffer, leaving it ready for use.

2.4. Electron paramagnetic resonance studies

Experiments were performed on a Bruker ELEXSYS E580 CW/Pulsed or a Bruker ELEXSYS-II E500 CW X-band equipped with an Oxford ESR900 helium flow cryostat using a Dual Mode Cavity (Bruker ER 4116DM). The bottom 10 mm of the sample column is carefully placed in the center of the resonator each time an experiment is performed. To do this reproducibly, the collar sealing the Kel-F rod that holds the sample column is never removed from it during a series of experiments. Since the collar attaches to the resonator's sample stack the sample itself is always held at the same vertical position. Correct sample placement is also visually inspected through the resonator window. Experimental conditions were typically: 100 kHz modulation frequency, 10 G modulation amplitude, 0.63 mW microwave power, and temperature set to 5 K. High-field/frequency measurements were carried out on a variable frequency/field broadband transmission spectrometer [31] at 406.4 GHz in a field ranging from 13.9 T to 14.9 T, 50 kHz modulation frequency, 1 or 25 G modulation amplitude and 0.2 or 2 mT/s sweep rates for high-resolution narrow sweeps and low-resolution wide sweeps, respectively, in a temperature range between 3 and 20 K. Simulated spectra were generated using the EasySpin toolbox in MATLAB [32].

2.5. Enzyme kinetic assay

The Michaelis–Menten parameters of the decarboxylase activity of free and resin-bound OxDC were determined through an end-point assay measuring the production of formate, as previously described [5,7,11]. 125 μL of protein-loaded IMAC resin (washed and centrifuged before re-suspension to remove any unbound enzyme) was mixed with 875 μL of starting buffer and constantly agitated to prevent sedimentation. Reactions were initiated in a 25 °C water bath by adding 10 μL of the slurry (or 1.5 μL of free WT OxDC for the control reaction) to 99 μL buffered oxalate solutions (acetate buffer at either pH 4.2 or pH 5.5). Low pH is expected to diminish the protein binding capacity of the resin because of increasing protonation of histidine ($pK_a \approx 6$). Experiments were therefore carried out at two pH values, 4.2 and 5.5. Similar reactions were conducted at both pH values using free WT

OxDC as the control.

2.6. Microscopy

50–100 μL of resin slurry were placed on a microscope slide and covered with a glass coverslip. A Zeiss PrimoVert microscope with various magnification levels ranging from 4 to 40 × was used to observe the resin beads before and after freeze-thaw cycles.

3. Results and discussion

3.1. Catalytic performance of the immobilized enzyme

Based on assays of the flow-through after protein loading, between 10 and 20 mg of enzyme was retained per mL of IMAC resin slurry. This number varied from experiment to experiment and is consistent with expectations based on the manufacturer's manual. Enzyme activity was measured at pH 4.0 and 5.5 and all kinetic parameters are reported in Table 1 (see Supplemental information, Fig. S1 for the experimental data). The data shows no effect of immobilization on the K_M values suggesting that the active site binding pocket is not directly affected by the resin. However, at both pH points an approximate 4-fold decrease in catalytic efficiency, $k_{cat}/K_{M.}$, was observed. This is likely due to steric crowding caused by immobilization as it becomes more difficult for the substrate to diffuse to active sites of OxDC. After 10 freeze-thaw cycles it can be seen that there is another approximate 4-fold decrease in activity with no effective change in K_M at pH 4.2. This may be explained in part by the partial loss of enzyme from the column after repeated freeze-thaw cycles. A loss in activity upon immobilization of OxDC on Eupergit C was also reported by Lin et al. [24]. It is exciting to see that different immobilization strategies lead to active enzyme. Immobilization of OxDC may lead to future applications in medical technology to detect and/or remove oxalate *in vivo* [33].

3.2. EPR experiments

EPR spectra were taken on immobilized as well as free OxDC in frozen solution at 5 K. The effective enzyme concentration was similar in both cases which led to similar EPR intensities.

Low-temperature X-band EPR spectra of OxDC show a strong transition near $g \approx 2$ and a weaker one near $g \approx 4$, both of which are split by hyperfine interaction with the ^{55}Mn nucleus with a coupling strength of approximately 90 G [7,12]. The $g \approx 4$ signal has been interpreted in the past as either a half-field signal of the main $g \approx 2$ center [12] or a second Mn(II) species with much higher zero field splitting [7]. The fact that its relative intensity compared to the main $g \approx 2$ sextet is variable for different preparations argues for the latter interpretation [12]. In fact, it might well be due to the xy_1 transition [34] of a C-terminal Mn(II) site with a fine structure parameter $|D|$ of the order of 4 GHz [15].

The two spectra in Fig. 1 look very similar. All EPR peaks seen in the free enzyme are reproduced in the spectrum of the immobilized sample with small variations in relative intensity. Since X-band EPR of Mn(II) is difficult to simulate for medium to large fine structure parameters, we used high-field EPR for further comparison. We interpret our spectra in terms of prior assignments made using high-field EPR on OxDC as a function of pH [15,16]. The corresponding EPR parameters are listed in Table 2. These experiments were initially performed at 3 K, the lowest temperature the helium flow cryostat was able to support, in order to focus on the transitions between the higher spin manifold, $m_S = -5/2 \leftrightarrow -3/2$ which are more sensitive to the magnitude of the fine structure than the central sextet transitions [15]. Fig. 2 demonstrates that the signals are comparable in shape and extent and clearly originate from the same species of Mn(II) with an approximate $D \approx -1.1$ GHz.

Similar agreement between free and immobilized enzyme was obtained in high-field EPR spectra performed with the sample poised at low pH giving rise to species A in the N-terminal site (see Supplemental information, Fig. S2). Fig. 3 shows the pH dependence of the central sextet of lines originating from the $m_S = -1/2 \leftrightarrow +1/2$ transitions taken at 20 K in high-resolution mode (modulation amplitude of 1 G). These signals reflect primarily species with small fine structure splitting $|D| < 1.5$ GHz, *i.e.*, the N-terminal Mn(II) [15]. In the case of the immobilized enzyme spectra were taken on the same sample, repeatedly frozen and thawed. The pH change was achieved by flushing the sample with buffer of the desired pH. For free enzyme small aliquots of base (potassium hydroxide) were added to the sample and the resulting pH measured between successive experiments. This leads to a small dilution effect for the free sample while the EPR intensity of the immobilized sample should potentially be free of dilution effects, although see below for intensity effects.

At high pH a single sextet pattern is observed and is identified

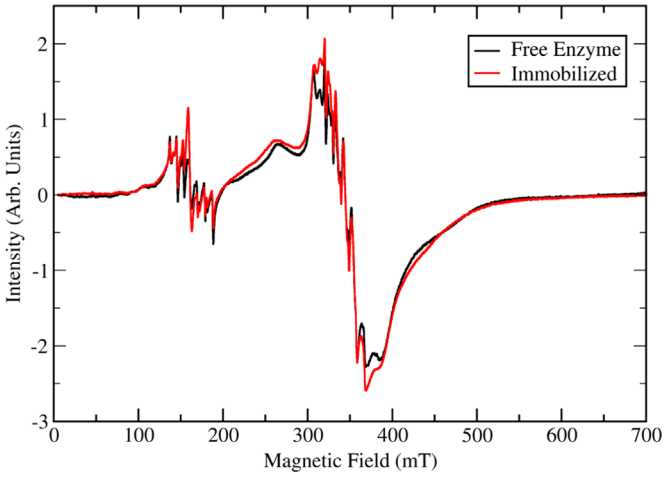

Fig. 1. Free (black trace) and Immobilized (red trace) WT-OxDC at 5 K. Instrumental parameters: 100 kHz modulation frequency, 10 G modulation amplitude, 0.63 mW microwave power.

Table 1
Michaelis–Menten kinetics of free and immobilized OxDC (pH in parentheses).

	Free OxDC (4.2)	Immobilized OxDC (4.2)	Free OxDC (5.5)	Immobilized OxDC (5.5)	Immobilized OxDC after 10 freeze-thaw cycles (4.2)
Enzyme concentration [μM]	7. 2 ± 0. 2	19. 1 ± 0. 4	7. 2 ± 0. 2	19. 1 ± 0. 4	10 ± 1
V_{max} [mM/s]	1. 13 ± 0. 09	1. 08 ± 0. 05	0. 076 ± 0. 005	0. 054 ± 0. 007	0. 12 ± 0. 03
V_{max} [U/mg]	215 ± 17	77 ± 4	14. 4 ± 0. 9	3. 9 ± 0. 5	16. 0 ± 4. 0
K_M [mM]	12 ± 3	16 ± 2	7 ± 1	8 ± 3	15 ± 7
k_{cat} [s^{-1}]	158 ± 13	56 ± 3	10. 6 ± 0. 7	2. 8 ± 0. 3	12 ± 3
k_{cat}/K_M [s^{-1} M^{-1}]	13000 ± 3000	3600 ± 500	1600 ± 300	400 ± 100	800 ± 400

as site B of the N-terminal Mn. At lower pH, low field shoulders appear in both data sets and may be interpreted as either of the two intermediate pH sites of the C-terminal Mn(II), M or X, observed by Tabares et al. [15]. As the pH is further lowered in the range of 4–6, the presence of a new species becomes evident due to the decrease in the zero-field splitting, specifically one or both of the mid pH C-terminal species that become prominent in the pH5 to pH6 range [15]. Simulations of these sites have been included in Fig. 3.

Upon closer inspection, the immobilized enzyme (Fig. 3, right panel) shows a slightly different trend compared to the free version. The intermediate site(s) become prominent at lower pH values compared to the free enzyme indicating a slightly different pH speciation. At present it is not clear what if any catalytic significance these intermediate pH sites have or whether their observation depends on the direction in which the pH is being changed (moving up as in our free enzyme sample, or moving down as in the immobilized preparation).

Experiments were carried out to detect the high pH C-terminal site H (see Supplemental information, Fig. S3). Its $|D|$ of approximately 10.7 GHz is so large because it corresponds to a less symmetric pentacoordinated Mn(II) similar to what has been seen in MnSOD [35]. It is observed in both the free and immobilized enzyme preparation.

Taken overall, both X-band and high-field EPR demonstrate that immobilization of OxDC has only minor spectral consequences paving the way for the use of immobilized enzyme to gather large EPR data sets where pH, redox potential, partial oxygen pressure, *etc*., are varied for the same sample over a large parameter range.

Table 2
Site specific zero field splitting parameters of Mn(II) sites in WT-OxDC [15].

Site	Species	pH range	g (iso)	A (MHz)	D (MHz)	E (MHz)
N-term	A	4–6	2.00088	252	−1350	230
N-term	B	7–9	2.00077	253	−1110	300
C-term	H	7–9	2.00080	250	10730	1700
C-term	X	5.5–7	2.00080	251	1400	340
C-term	M	4.5–6.5	2.00080	251	−1500	450
C-term	L	4–4.5	2.00086	251	4170	720
C-term	L2	4	2.00078	252	5060	250

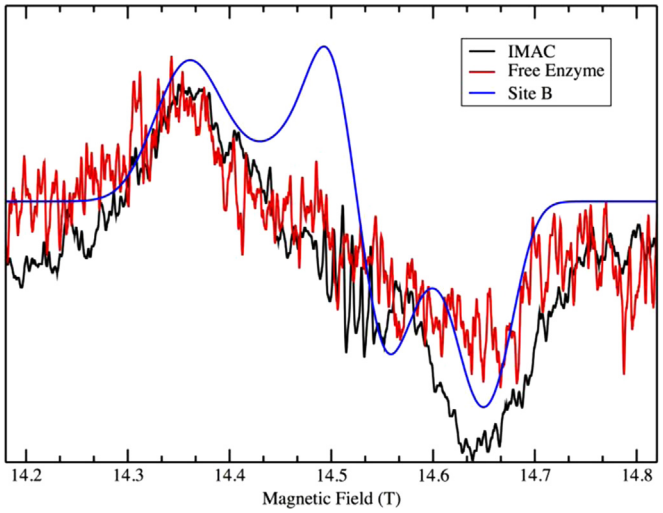

Fig. 2. 406.4 GHz HF-EPR at 3 K of free enzyme at pH 8.42 (red) and immobilized at pH 8.50 (black). The simulation (blue) is based on parameters of site B by Tabares et al. [15] Instrumental parameters: 50 kHz modulation frequency, 25 G modulation amplitude, 2 mT/s sweep rate. Simulation parameters: $g=2.00077$, $A=253$ MHz, $D=-1100$ MHz, $E=300$ MHz.

3.3. Freeze-thaw effects

In principle, immobilization allows to reuse the same sample while changing the external conditions for the protein. However, protein retention may become an issue upon repeated wash cycles because His_6-tag binding to the resin is an equilibrium. The mechanical integrity of the polystyrene resin beads may also be compromised upon repeated freeze-thaw cycles with unwanted side effects. We performed control experiments where loaded resin was subjected to repeated freeze-thaw-wash cycles while monitoring the low temperature EPR signals and taking aliquots to observe any damage to the beads under a microscope. Between each freeze thaw cycle, 10 column volumes of starting buffer was flowed through the column. The flow-through was saved and analyzed for protein released utilizing the Bradford assay. The amount of protein remaining on the column was calculated and is reported in Table 3 (Fig. S4).

The sample experiences a steady decrease of protein upon repeated freeze-thaw-wash cycles. Surprisingly, the EPR intensity is increasing throughout this sequence. We checked that Mn(II) itself is not retained on the resin, excluding the possibility of denatured protein leaving its Mn behind (Fig. S5). Since the X-band EPR spectrum is not significantly changed upon subsequent freeze-thaw cycles, we can exclude changes in Mn coordination induced by the process.

Fig. 4 shows representative micrographs of the resin before and

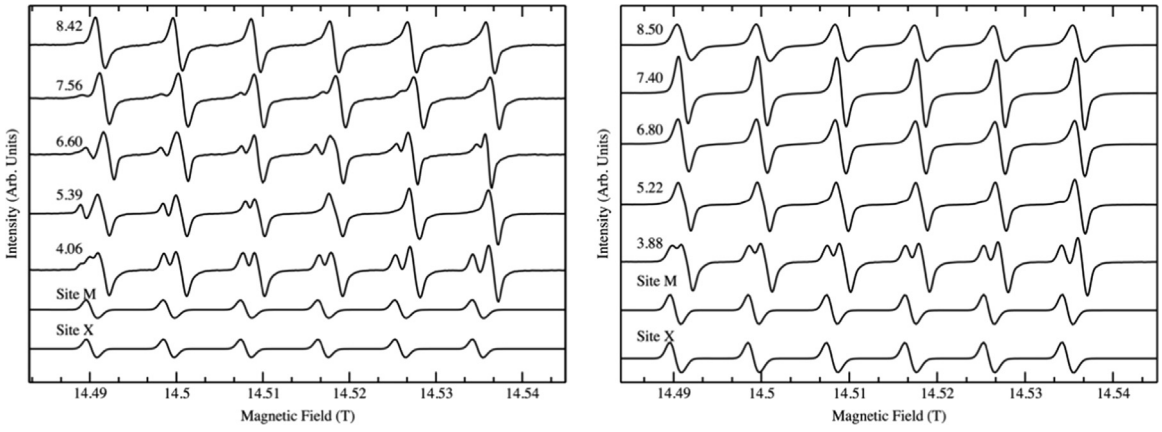

Fig. 3. pH dependence of the 406.4 GHz HF-EPR at 20 K spectra of free enzyme (left panel), immobilized (right panel). Simulations for sites M and X are shown at the bottom. Instrumental parameters: 50 kHz modulation frequency, 1 G modulation amplitude, 0.2 mT/s sweep rate.

after freezing.

Fresh IMAC Profinity resin kept at 4 °C consists of spherical polymeric UNOsphere beads of various sizes between 51 and 63 μm. In Fig. 4A and C, micrographs of the resin beads are shown under 20×, and 4× magnification. Prior to freezing the beads exhibit a consistent spherical shape. After several cycles, the beads show significant fracturing as seen in Fig. 4B (black arrows) and 4D. Many of the large beads are broken into smaller, misshapen pieces, and could potentially lead to higher surface area and tighter packing on the column. These smaller pieces may settle at the bottom of the column extending into the sensitive part of our rectangular TE102 resonator (approximately the central 10 mm), affording higher protein density. This breakage is expected due to the brittleness of the polystyrene beads. The changes in resin morphology may also explain the gradual loss of enzyme over the course of various freeze-thaw cycles since very small fragments may not be retained by the 5 μm filter. A small increase in the EPR intensity may also be explained by the magnetic dilution that comes with lower enzyme concentration due to losses after multiple freeze-thaw-flush cycles.

Our experiments on OxDC have demonstrated that the N-terminal His_6-tag can be used to immobilize OxDC while preserving catalytic activity. The advantage of this method is that no further chemical step is needed for immobilization. Similar effective enzyme concentrations as with free enzyme in solution are obtained. The solid support allows use of a flow column where enzyme can be reused multiple times in a given experiment while external conditions such as pH are varied. The method is not recommended for quantitative EPR at cryogenic temperatures because repeated freeze-thaw-wash cycles lead to fracturing of resin beads, loss of enzyme from the column, and EPR signal enhancement due to denser packing of the fractured beads. We are currently exploring alternative immobilization techniques for quantitative EPR [36].

Table 3
Total protein on IMAC resin after initial loading and subsequent freeze-thaw cycles.

Freeze-thaw cycles	IMAC-bound OxDC (mg)
0	13.7
1	10.9
2	9.9
3	8.9
4	8.4
5	7.7
6	7.0

Acknowledgments

Funding for this work was provided by the National Science Foundation under Grant CHE-1213440. The high-field EPR spectra were recorded at the NHMFL, which is funded by the NSF through the Cooperative Agreement no. DMR-1157490, the State of Florida and the U.S. DOE. A plasmid containing the gene encoding C-terminally, His_6-tagged wild-type *Bacillus subtilis* OxDC was generously provided by Dr. Stephen Bornemann (John Innes Centre, Norwich, UK). Useful technical discussions with Dr. Nigel G. J. Richards (Dept. of Chemistry and Chemical Biology, Indiana University – Purdue University, Indianapolis) are gratefully acknowledged.

Appendix A. Supplementary material

Supplementary data associated with this article can be found in the online version at http://dx.doi.org/10.1016/j.bbrep.2015.08.017.

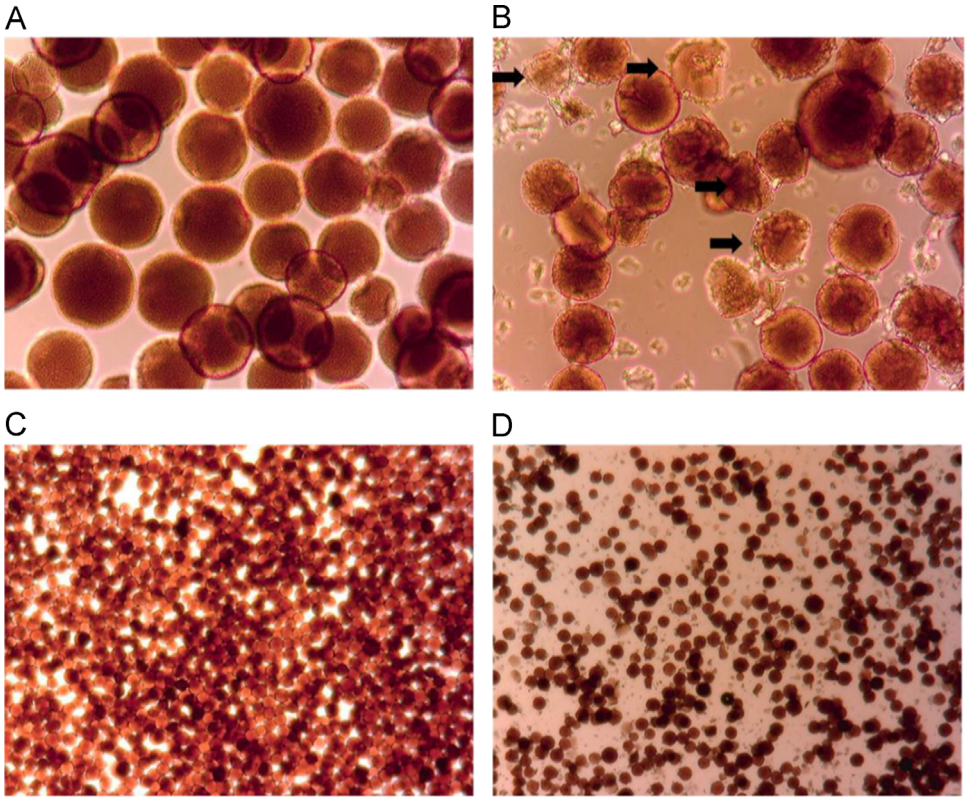

Fig. 4. Comparison of fresh, unfrozen, Zn-loaded resin observed under 20× (A) and 4× magnification (C), and OxDC-loaded resin exposed to 6 freeze-thaw-wash cycles observed under 20× (B) and 4× magnification (D).

References

[1] J. Dunwell, Cupins: a new superfamily of functionally diverse proteins that include germins and plant storage proteins, Biotechnol. Genetic Eng. Rev. 15 (1998) 1–32.
[2] J. Dunwell, A. Purvis, S. Khuri, Cupins: the most functionally diverse protein superfamily? Phytochemistry 65 (2004) 7–17.
[3] S. Khuri, F.T. Bakker, J.M. Dunwell, Phylogeny, function, and evolution of the cupins, a structurally conserved, functionally diverse superfamily of proteins, Mol. Biol. Evol. 18 (2001) 593–605.
[4] R. Anand, P. Dorrestein, C. Kinsland, T. Begley, S. Ealick, Structure of oxalate decarboxylase from *Bacillus subtilis* at 1.75 Å resolution, Biochemistry 41 (2002) 7659–7669.
[5] V.J. Just, C.E.M. Stevenson, L. Bowater, A. Tanner, D.M. Lawson, S. Bornemann, A closed conformation of *Bacillus subtilis* oxalate decarboxylase OxdC provides evidence for the true identity of the active site, J. Biol. Chem. 279 (2004) 19867–19874.
[6] V.J. Just, M.R. Burrell, L. Bowater, I. McRobbie, C.E.M. Stevenson, D.M. Lawson, S. Bornemann, The identity of the active site of oxalate decarboxylase and the importance of the stability of active-site lid conformations, Biochem. J. 407 (2007) 397–406.
[7] A. Tanner, L. Bowater, S. Fairhurst, S. Bornemann, Oxalate decarboxylase requires manganese and dioxygen for activity-overexpression and characterization of *Bacillus subtilis* YvrK and YoaN, J. Biol. Chem. 276 (2001) 43627–43634.
[8] D. Svedruzic, S. Jonsson, C. Toyota, L. Reinhardt, S. Ricagno, Y. Linqvist, N. Richards, The enzymes of oxalate metabolism: unexpected structures and mechanisms, Arch. Biochem. Biophys. 433 (2005) 176–192.
[9] E. Moomaw, A. Angerhofer, P. Moussatche, A. Ozarowski, I. García-Rubio, N. Richards, Metal dependence of oxalate decarboxylase activity, Biochemistry 48 (2009) 6116–6125.
[10] U.T. Twahir, C.N. Stedwell, C.T. Lee, N.G.J. Richards, N.C. Polfer, A. Angerhofer, Observation of superoxide production during catalysis of *Bacillus subtilis* oxalate decarboxylase at pH 4, Free Radic. Biol. Med. 80 (2015) 59–66.
[11] P. Campomanes, W.F. Kellett, L.M. Easthon, A. Ozarowski, K.N. Allen, A. Angerhofer, U. Rothlisberger, N.G.J. Richards, Assigning the EPR fine structure parameters of the Mn(II) centers in *Bacillus subtilis* oxalate decarboxylase by site-directed mutagenesis and DFT/MM calculations, J. Am. Chem. Soc. 136 (2014) 2313–2323.
[12] C. Chang, D. Svedruzic, A. Ozarowski, L. Walker, G. Yeagle, R. Britt, A. Angerhofer, N. Richards, EPR spectroscopic characterization of the manganese center and a free radical in the oxalate decarboxylase reaction – identification of a tyrosyl radical during turnover, J. Biol. Chem. 279 (2004) 52840–52849.
[13] W. Imaram, B. Saylor, C. Centonze, N. Richards, A. Angerhofer, EPR spin trapping of an oxalate-derived free radical in the oxalate decarboxylase reaction, Free Radic. Biol. Med. 50 (2011) 1009–1015.
[14] M. Moral, C. Tu, W. Imaram, A. Angerhofer, D. Silverman, N. Richards, Nitric oxide reversibly inhibits *Bacillus subtilis* oxalate decarboxylase, Chem. Commun. 47 (2011) 3111–3113.
[15] L. Tabares, J. Gatjens, C. Hureau, M. Burrell, L. Bowater, V. Pecoraro, S. Bornemann, S. Un, pH-dependent structures of the manganese binding sites in oxalate decarboxylase as revealed by high-field electron paramagnetic resonance, J. Phys. Chem. B 113 (2009) 9016–9025.
[16] A. Angerhofer, E.W. Moomaw, I. García-Rubio, A. Ozarowski, J. Krzystek, R. T. Weber, N.G.J. Richards, Multifrequency EPR Studies on the Mn(II) centers of oxalate decarboxylase, J. Phys. Chem. B 111 (2007) 5043–5046.
[17] E. Hochuli, W. Bannwarth, H. Döbeli, R. Gentz, D. Stüber, Genetic approach to facilitate purification of recombinant proteins with a novel metal chelate adsorbent, Nat. Biotechnol. (1988) 1321–1325.
[18] V. Gaberc-Porekar, V. Menart, Perspectives of immobilized-metal affinity chromatography, J. Biochem. Biophys. Methods 49 (2001) 335–360.
[19] A.C. Chikere, B. Galunsky, V. Schünemann, V. Kasche, Stability of immobilized soybean lipoxygenases: influence of coupling conditions on the ionization state of the active site Fe, Enzyme Microb. Technol. 28 (2001) 168–175.
[20] G. Jack, Immunoaffinity chromatography, Mol. Biotechnol. 1 (1994) 59–86.
[21] P.A. Fiorito, S.I. Córdoba de Torresi, Optimized multilayer oxalate biosensor, Talanta 62 (2004) 649–654.
[22] C.A. Malpass, K.W. Millsap, H. Sidhu, L.B. Gower, Immobilization of an oxalate-degrading enzyme on silicone elastomer, J. Biomed. Mater. Res. 63 (2002) 822–829.
[23] K.G. Raghavan, U. Tarachand, Degradation of oxalate in rats implanted with immobilized oxalate oxidase, FEBS Lett. 195 (1986) 101–105.
[24] R. Lin, R. Wu, X. Huang, T. Xie, Immobilization of oxalate decarboxylase to Eupergit and properties of the immobilized enzyme, Prep. Biochem. Biotechnol. 41 (2011) 154–165.
[25] A. Bhardwaj, J. Lee, K. Glauner, S. Ganapathi, D. Bhattacharyya, D.A. Butterfield, Biofunctional membranes: an EPR study of active site structure and stability of papain non-covalently immobilized on the surface of modified poly(ether) sulfone membranes through the avidin-biotin linkage, J. Membr. Sci. 119 (1996) 241–252.
[26] D.A. Butterfield, D. Bhattacharyya, S. Daunert, L. Bachas, Catalytic biofunctional membranes containing site-specifically immobilized enzyme arrays: a review, J. Membr. Sci. 181 (2001) 29–37.
[27] Y. Chen, R. Pasquinelli, M. Ataai, R.R. Koepsel, R.A. Kortes, R.E. Shepherd, Coordination of two high-affinity hexamer peptides to copper(II) and palladium (II) models of the peptide – metal chelation site on IMAC resins, Inorg. Chem. 39 (2000) 1180–1186.
[28] C. Garcia-Galan, Á. Berenguer-Murcia, R. Fernandez-Lafuente, R.C. Rodrigues, Potential of different enzyme immobilization strategies to improve enzyme performance, Adv. Synth. Catal. 353 (2011) 2885–2904.
[29] G.A. Marg, G.L. Millhauser, P.S. Skerker, D.S. Clark, Application of EPR methods in studies of immobilized enzyme systemsa, Ann. N. Y. Acad. Sci. 469 (1986) 253–258.
[30] B.T. Saylor, L.A. Reinhardt, Z. Lu, M.S. Shukla, L. Nguyen, W.W. Cleland, A. Angerhofer, K.N. Allen, N.G.J. Richards, A structural element that facilitates proton-coupled electron transfer in oxalate decarboxylase, Biochemistry 51 (2012) 2911–2920.
[31] A. Ozarowski, S.A. Zvyagin, W.M. Reiff, J. Telser, L.-C. Brunel, J. Krzystek, High-frequency and -field EPR of a pseudo-octahedral complex of high-spin Fe(II): Bis(2,2′-bi-2-thiazoline)bis(isothiocyanato)iron(II), J. Am. Chem. Soc. 126 (2004) 6574–6575.
[32] S. Stoll, A. Schweiger, EasySpin, a comprehensive software package for spectral simulation and analysis in EPR, J. Magn. Res. 178 (2006) 42–55.
[33] J.D. Watterson, P.A. Cadieux, D.T. Beiko, A.J. Cook, J.P. Burton, R.R. Harbottle, C. Lee, E. Rowe, H. Sidhu, G. Reid, J.D. Denstedt, Oxalate-degrading enzymes from oxalobacter formigenes: a novel device coating to reduce urinary tract biomaterial-related encrustation, J. Endourol. 17 (2003) 269–274.
[34] T.C. DeVore, R.J. Van Zee, W. Weltner, High spin molecules: ESR of MnF and MnF_2 at 4 °K, J. Chem. Phys. 68 (1978) 3522–3527.
[35] S. Un, L.C. Tabares, N. Cortez, B.Y. Hiraoka, F. Yamakura, Manganese(II) zero-field interaction in cambialistic and manganese superoxide dismutases and its relationship to the structure of the metal binding site, J. Am. Chem. Soc. 126 (2004) 2720–2726.
[36] L.J. Bailey, K.M. Sheehy, R.J. Hoey, Z.P. Schaefer, M. Ura, A.A. Kossiakoff, Applications for an engineered Protein-G variant with a pH controllable affinity to antibody fragments, J. Immunol. Methods 415 (2014) 24–30.